Pure Appl. Geophys.

https://doi.org/10.1007/s00024-025-03788-x

Pure and Applied Geophysics

Enhanced Drought Vulnerability in the Kızılırmak Basin: Understanding the Influence of Climate Models

Musa Esit,[1] Mehmet Ishak Yuce,[2] Islam Yasa,[3] and Ibrahim Halil Deger[4]

Abstract—This research examines how significant atmospheric fluctuations affect drought conditions, in the Kızılırmak Basin in Türkiye. We studied the impact of climate indices like NAO, Niño, AMO, PDO, ONI, and SOI by using the Standardized Precipitation Evapotranspiration Index (SPEI) as an indicator of drought. The findings reveal an increase in both the frequency and severity of droughts after 2015. In the 2000s, short-term droughts lasted from 1 to 3 months. However, after 2020, longer-term droughts lasting between 6 and 24 months have become more severe. Correlation and lead-time analyses reveal ENSO indices, particularly Niño 3.4 and ONI, as primary drivers of drought, with a positive impact. The SOI emerged as a significant predictor of future drought conditions. While PDO and AMO influence drought, their effects are less pronounced. Understanding these complex relationships is crucial for developing effective regional drought management strategies.

Keywords: Kızılırmak Basin, Drought, SPEI, ENSO, NAO, AMO, PDO, SOI, Atmospheric oscillations, Climate variability.

1. Introduction

Large-scale and prolonged droughts, the hallmark of climate extremes, cause enormous economic hardship and trigger water scarcity and food insecurity, with widespread consequences (Abdelkader & Yerdelen, 2022; Hamal et al., 2021; Ullah et al., 2023; Wilhite, 2000). This phenomenon usually appears as extended dry periods based on below-average precipitation and other thermodynamic factors (AghaKouchak et al., 2015; Mishra & Singh, 2010). It is the most widespread climate extreme, impacting more people globally than any other, particularly in semi-arid areas (Afshar et al., 2020; Wilhite, 2005). Additionally, it significantly impacts agriculture, land cover, soil moisture levels, and surface and groundwater resources (Esit et al., 2021; Oñate-Valdivieso et al., 2020). Wilhite and Glantz (1985) categorized drought into four main types based on how it develops and impacts various areas: meteorological, hydrological, agricultural, and socioeconomic.

Different types of drought indicators such, as those related to agricultural, meteorological, hydrologic, and socio-economic factors are commonly used globally to monitor instances of drought and provide insights, for minimizing drought risks and managing their consequences (He et al., 2024; Meresa et al., 2023; Wang et al., 2023; Yuce et al., 2023). The Standardized Precipitation Index (SPI) by McKee et al. (1993) is one of the drought measures researchers use. It's easy to work with because it needs rainfall data and can adapt to different periods. Other common indexes include the Palmer Drought Severity Index (PDSI) (Palmer, 1965), the Standardized Runoff Index (SRI) (Shukla & Wood, 2008), the Standardized Soil Moisture Index (SSI) (Hao & AghaKouchak, 2013), and the Standardized Precipitation Evapotranspiration Index (SPEI) (Vicente-Serrano et al., 2010). Researchers often employ the SPEI to assess and forecast droughts on a global scale (Ghasemi et al., 2021; Karbasi et al., 2022; Nejadrekabi et al., 2022; Peng et al., 2020). The SPEI also helps to examine various drought types (Danandeh Mehr & Vaheddoost, 2020; Gumus, 2023; Li et al., 2020; Pei et al., 2020).

Climate signals, ocean-atmospheric oscillations, and atmospheric phenomena like rainfall, streamflow,

[1] Civil Engineering Department, Adiyaman University, Adiyaman, Türkiye. E-mail: mesit@adiyaman.edu.tr
[2] Civil Engineering Department, Gaziantep University, Gaziantep, Türkiye.
[3] Civil Engineering Department, Ondokuz Mayis University, Samsun, Türkiye.
[4] Civil Engineering Department, Hasan Kalyoncu University, Gaziantep, Türkiye.

Published online: 21 July 2025

and severe droughts offer many opportunities to study and forecast droughts and other climate-related risks (Aghelpour et al., 2023; Mohammadrezaei et al., 2020). Climate signals, ocean-atmospheric oscillations, and atmospheric phenomena like rainfall, streamflow, and severe droughts offer many opportunities to study and forecast droughts and other climate-related risks (Aghelpour et al., 2023; Mohammadrezaei et al., 2020). Teleconnection pattern refers to the interaction between the atmosphere and the ocean which produce climate links over long distances. These connections can last from weeks to decades and allow us to predict climate patterns from yearly to decades (Mohammadrezaei et al., 2023; Sureh et al., 2024). So it's essential to have a deep understanding of teleconnection patterns and how they interact with climatological, hydrological, agricultural and biological systems (Manzano et al., 2019; Molla, 2020; Nourani et al., 2021; Yao et al., 2019, 2024). Teleconnection patterns which are the connection between oceanic-atmospheric oscillations and sea surface temperature (SST) provide prognostic information and have been associated with drought scenarios in many places around the world (Murgulet et al., 2017; Ndehedehe, 2022; Sagarika et al., 2015). The main forms of natural climate variability are the Pacific basin fluctuations, namely the Pacific Decadal Oscillation (PDO) and El Niño-Southern Oscillation (ENSO), and the Atlantic basin fluctuations, particularly the Atlantic Multidecadal Oscillation (AMO) (Chylek et al., 2014; Liu & Di Lorenzo, 2018). Mohammadrezaei et al. (2020) looked at the relationship between the Arctic Oscillation (AO) and drought in Iran. They found a statistically significant relationship between the AO and drought all over the country. Also, their study showed a relationship between the AMO and Niño (3 + 4) indices and dryness in the western and northern parts of Iran, respectively. During an investigation into the relationship between the North Atlantic Oscillation (NAO) and winter precipitation in Hungary, Matyasovszky (2003) found that the NAO was in its warm phase (positive) during drought and in its cold phase (negative) during wet periods. Gu et al. (2024) found that there was a significant decline in terrestrial water storage (TWS) over China from 2002 to 2021. The group of atmospheric circulation indices known as the Western Pacific and Indian Ocean (WPIO) has the most impact on TWS fluctuations. The sea surface temperature anomalies in the NINO 3.4 region and the Western Pacific Warm Pool area index had a significant positive relationship with TWS in southern China. Fan et al. (2024) found that ENSO had the most impact on drought in the Lancang-Mekong River Basin. The sensitivity to drought was in the order of ENSO > AO > NAO > PDO. Zhang et al. (2024) showed that the hot and dry conditions in summer in Xinjiang are greatly influenced by the abnormal sea surface temperatures in the North Atlantic, namely the tripole pattern. These abnormal temperatures cause a wave-like pattern that affects the circulation of the atmosphere in the region. Rezaei (2023) found that drought in the Middle East and North Africa (MENA) region is driven by the Pacific Decadal Oscillation (PDO), El Niño-Southern Oscillation (ENSO) and Atlantic Multidecadal Oscillation (AMO), and the North Atlantic Oscillation (NAO). The impacts of these oscillations on drought vary by timescale. Yang et al. (2020) found that from 1950 to 2016 southwestern Canada got drier in winter. But across the whole country the frequency, extent and severity of droughts decreased. These changes were found to be related to changes in climate indices such as ENSO, PDO, AMO, and AO over time.

Türkiye's geographical location within a semi-arid climatic zone predisposes it to frequent drought occurrences. In light of projected climate change scenarios, particularly those involving extreme temperature distributions, it is anticipated that Türkiye will experience alterations in both the intensity and temporal extent of drought events (Turan, 2017). Türkeş (2020) identified several significant drought periods in Turkey over the past 40 years, with the most severe occurring in 1971–1974, 1983–1984, 1989–1990, 1996–2001, and 2007–2008, often evolving from meteorological to agricultural and hydrological droughts (Kurnaz, 2014; Türkeş & Erlat, 2003). In addition, according to NASA Earth Observatory (2021), Türkiye faced extensive severe drought conditions in early 2021, with Istanbul's reservoir levels plummeting to 15-year lows, posing significant risks to agricultural productivity. Numerous studies have been conducted in Türkiye regarding

teleconnection climate indices and hydrometeorological parameters. For example, teleconnection of atmospheric oscillations on streamflow (Kebapcioğlu & Partal, 2024; Sezen, 2024; Yılmaz & Tosunoğlu, 2023), precipitation (Baltacı et al., 2018; Duzenli et al., 2018; Kömüşçü & Aksoy, 2024; Türkeş & Erlat, 2005), hydrological drought (Tosunoglu et al., 2023; Vazifehkhah & Kahya, 2019) are investigated.

However, despite its critical importance, meteorological drought has not been examined in detail across Türkiye, particularly concerning the influence of large-scale atmospheric oscillation indices. This significant knowledge gap hinders a comprehensive understanding of drought dynamics and limits the efficacy of drought mitigation strategies in the region. In light of this, the present study aims to fill this void by investigating the effects of various atmospheric oscillation indices on drought occurrences within the Kızılırmak basin, one of Türkiye's most vital hydrological systems. Specifically, this research seeks to: (1) identify the relationships between major atmospheric-oceanic teleconnections and drought periods at multiple temporal scales within the Kızılırmak basin, and (2) analyze how these relationships vary over different timeframes.

2. Study Area and Data

Kızılırmak Basin is an important water resource in Türkiye. Located between 37°58′ to 41°44′ north and 32°48′ to 38°22′ east, it is 3.5% of Türkiye's total water (Arslan et al., 2016; Robleh et al., 2024). Its annual water flow is 6.48 billion m^3, the second biggest water basin in Turkey after the Euphrates. The basin has undulating topography, more pronounced in northern and eastern parts where the mountainous landscape prevails. The hydrological system of the basin is defined by the Kızılırmak River and its tributaries which form the main water catchment areas (Terzi & İlker, 2021). Basin covers an area of 78.180 km2, 3.528.800 ha of which are alluvial plains which is a significant part of the basin's arable land and agricultural potential. The basin has a continental climate. This climate is characterized by extreme seasonal changes, winters with heavy snow and hot summers. Annual precipitation is between 400 and 600 mm, a moderate amount that affects the region's hydrology and ecosystems (Akturk et al., 2022; Citakoglu & Minarecioglu, 2021; Deger et al., 2023). The Kızılırmak Basin has a complex hydrological network with various aquatic ecosystems and anthropogenic water management structures. Kızılırmak Basin, an important water resource for Türkiye, needs to be conserved and managed sustainably to be long-term viable and ecological integrity (Öztürk et al., 2023). The distribution of the meteorological stations used in the basin is given in Fig. 1. Also, Table 1 shows the information about 14 meteorological stations used in the study. The longest meteorological record was measured at stations 17,160 Kirsehir and 17,196 Kayseri, shortest record was measured at station 17,833 Avanos. Data points are taken from different parts of the basin to make basin-wide generalizations. Precipitation data, a crucial variable in this study, were directly obtained from the Turkish General Directorate of Meteorology (MGM). The MGM operates a comprehensive network of meteorological stations across Turkey, ensuring standardized and quality-controlled data collection. Further details on the challenges and accuracy considerations in precipitation measurements, including discussions on various instrumentation and potential error sources, can be found in comprehensive reviews such as Gultepe et al. (2017) and (2019) papers.

3. Methodology

3.1. Standardized Precipitation Evapotranspiration Index (SPEI)

The Standardized Precipitation Evapotranspiration Index (SPEI) developed by Vicente-Serrano et al. (2010) is more comprehensive than the Standardized Precipitation Index (SPI). By including both precipitation and evapotranspiration, the SPEI takes into account the temperature impact on drought. This allows for a more detailed analysis of drought intensity, duration, and severity at different time scales and regions (Ghasemi et al., 2021). The SPEI is calculated based on the non-exceedance probability of the difference between precipitation and potential

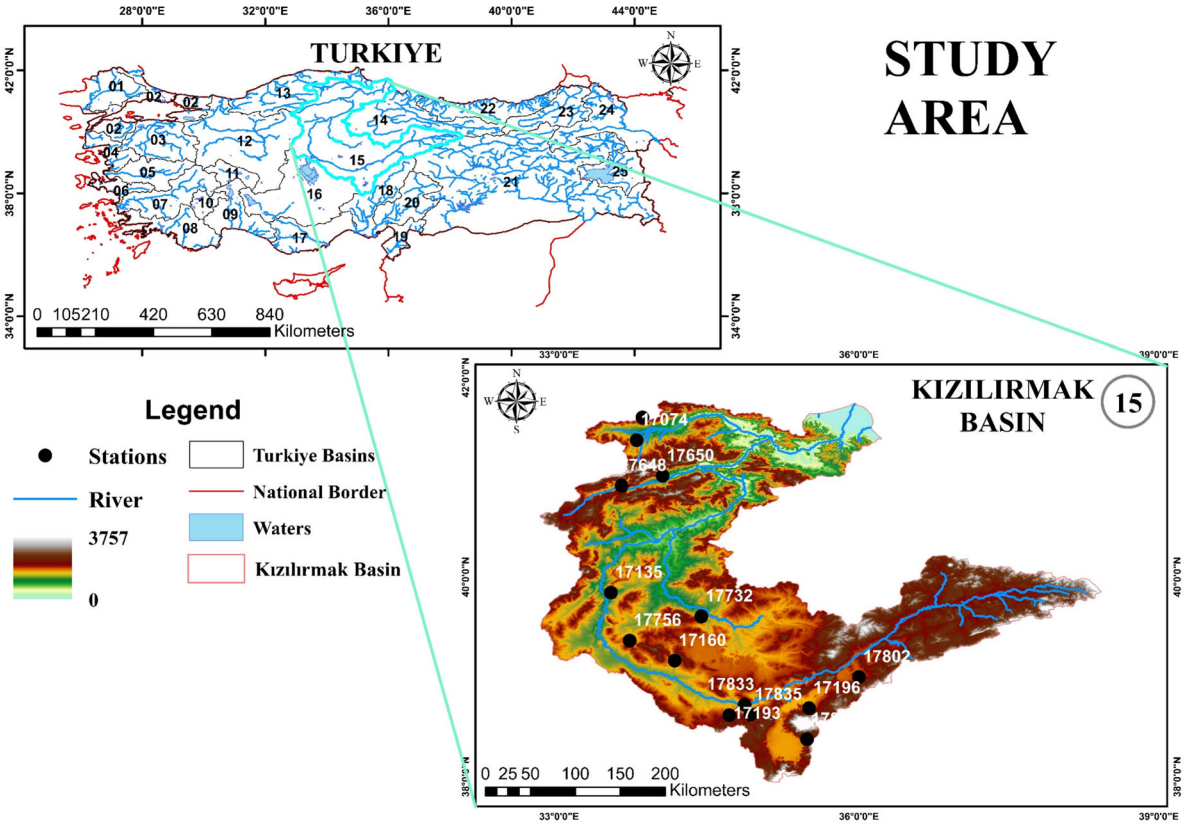

Fig. 1
The geomorphological characteristics of the Kızılırmak Basin and the spatial distribution of monitoring stations within its boundaries

Table 1

The location and recording information of the meteorological stations used in this study

Station Number	Station Name	Latitude	Longitude	Altitude	Earliest Record Year	Latest Record Year
17,074	Kastamonu	41.371	33.7756	800	1951	2020
17,135	Kirikkale	39.843	33.5181	751	1963	2021
17,160	Kirsehir	39.164	34.1561	1007	1951	2021
17,193	Nevsehir	38.616	34.7025	1260	1959	2021
17,196	Kayseri	38.687	35.5	1094	1951	2021
17,618	Devrekani	41.599	33.834	1050	1977	2021
17,648	Ilgaz	40.915	33.625	885	1969	2021
17,650	Tosya	41.013	34.036	870	1959	2021
17,732	Cicekdag	39.607	34.4235	900	1971	2021
17,756	Kaman	39.365	33.706	1075	1965	2020
17,802	Pinarbasi	39	36	1542	1963	2021
17,833	Avanos	38.722	34.856	950	1986	2021
17,835	Urgup	38.622	34.9144	1068	1972	2021
17,836	Develi	38.374	35.4797	1204	1965	2021

evapotranspiration. This difference is then calibrated using a three-parameter log-logistic probability distribution function. The use of this distribution is important because it can handle negative values which are common in the water balance calculations of the SPEI methodology. This statistical approach allows the SPEI to normalize the climatic water balance over different time scales so that we can compare different regions and periods (Tirivarombo et al., 2018; Vicente-Serrano et al., 2010). The SPEI is calculated by normalizing the climatic water balance using Log-logistic distribution. In this study, the Potential Evapotranspiration (PET) is calculated using the Thornthwaite method (Thornthwaite, 1948). The main calculation is to find the difference (Di) between precipitation (P) and PET for a month (i), as shown in Eq. (2). This approach allows us to have a standardized representation of water surplus or deficit, taking into account both water input and atmospheric water demand. The Thornthwaite method calculates Potential Evapotranspiration using temperature as the only input parameter.

$$PET = 16d\left(\frac{10T}{I}\right)^{a} \tag{1}$$

where; T is the monthly mean temperature (°C), and d is a correction factor for diurnal duration variation across months. d is calculated from standard tables which are calibrated to the latitude of the study area. I and i are the annual and monthly heat indices respectively.

$$D_i = P_i - PET_i \tag{2}$$

The D values are summed across time scales.

$$D_n^k = \sum_{i-0}^{k-1} P_{n-1} - (PET)_{n-1} \tag{3}$$

where k is the aggregation period in months and n is the calculation month. The log-logistic probability density function is:

$$f(x) = \frac{\beta}{\alpha}\left(\frac{x-y}{a}\right)^{\beta-1}\left(1+\left(\frac{x-y}{a}\right)^{\beta}\right)^{-2} \tag{4}$$

with α, β, and γ as scale, shape, and origin parameters ($\gamma > D < \infty$), the probability distribution function for the D series is:

$$f(x) = \left[1+\left(\frac{a}{x-y}\right)^{\beta}\right]^{-1} \tag{5}$$

The SPEI is derived from standardizing F(x) values using the Abramowitz and Stegun (1968) method.

$$SPEI = W - \frac{C_0 + C_1 W + C_2 W^2}{1 + d_1 W + d_2 W^2 + d_3 W^3} \tag{6}$$

$$W = \sqrt{-2In(P)} for P \leq 0.5 \tag{7}$$

where $C_0 = 2.515517$, $C_1 = 0.802853$, $d_1 = 1.432788$, $d_2 = 0.189269$, $d_3 = 0.001308$.

3.2. Pearson Correlation, Cross-Correlation and Cross-Wavelet Transform (XWT)

Correlation analysis measures the relationship between variables with a coefficient commonly used in climate research. This is expressed numerically by the correlation coefficient which gives a standardised measure of the strength and direction of the linear relationship between the variables (Benesty et al., 2009). The Pearson product-moment correlation coefficient (PPMCC) was used to look at the concurrent interdependence between drought indices and oceanic-atmospheric circulation patterns across multiple time scales (Yang & Xing, 2022). This statistical method allows us to quantify the linear relationships between these climate variables and assess potential teleconnections and their temporal variability. Correlations were tested for significance using a Student's t-test at a 95% confidence level. The sample correlation coefficient, r, between X and Y is:

$$r = \frac{\sum_{i=1}^{n}(X_i - \overline{X})(Y_i - \overline{Y})}{\sqrt{\sum_{i=1}^{n}(X_i - \overline{X})^2}\sqrt{\sum_{i=1}^{n}(Y_i - \overline{Y})^2}} \tag{8}$$

Xi and *Yi* represent the SPEI and ocean-atmospheric circulation indices, respectively, where i is the individual data point. $\overline{X}$ and $\overline{Y}$ are the mean values of *Xi* and *Yi*. The correlation coefficient, r, ranges from − 1 to 1. A positive r ($r > 0$) means positive correlation, a negative r ($r < 0$) means negative correlation (Zhong et al., 2017).

Cross-correlation looks at how similar two variables are over time, considering the time lag between them. This method shows how one variable correlates with the past values of another. Unlike simple correlation, cross-correlation can look at relationships at different time offsets, before and after, to give a more complete picture of the relationship between variables (Qian et al., 2015). The CCF can be calculated by:

$$r_k = \frac{\widehat{C}_K(x,y)}{\widehat{\delta}_x \widehat{\delta}_{y+k}} \tag{9}$$

the sample covariance is denoted by $\widehat{C}_K$ (x, y), and the sample mean square deviations, $\widehat{\delta}_x$ and $\widehat{\delta}_{y+k}$, are calculated as follows:

$$\begin{cases} \widehat{C}_K = \frac{1}{n-k}\sum_{i=1}^{n-k}(x_i - \overline{x})\left(y_{i+k} - \overline{y}_{i+k}\right) \\ \widehat{\delta}_x = \left[\frac{1}{n-k}\sum_{i=1}^{n-k}(x_i - \overline{x})^2\right]^{\frac{1}{2}} \\ \widehat{\delta}_{y+k} = \left[\frac{1}{n-k}\sum_{i=1}^{n-k}\left(y_{i+k} - \overline{y}_{i+k}\right)^2\right]^{\frac{1}{2}} \end{cases} \tag{10}$$

To examine the connection between pairs of time-domain signals, *xn* and *yn*, the Cross Wavelet Transform (XWT) is employed. This is computed as:

$$W^{XY} = W^X W^{Y*} \tag{11}$$

where * represents complex conjugation, the cross-wavelet power is defined as the absolute value of $\left|W^{XY}\right|$. The phase angle, or argument, arg (W^{XY}) indicates the local phase difference between *xn* and *yn* within the time–frequency plane. The theoretical distribution of cross wavelet power for two time series with background power spectra P_k^X and P_k^Y is detailed in reference Torrence and Compo (1998). The WCOH, a measure of time–frequency coherence, is calculated using the method outlined in Torrence and Webster (1999).

$R_n^2(s) = \frac{\left|S\left(s^{-1}W_n^{XY}(s)\right)\right|^2}{S\left(s^{-1}W_n^X(s)^2\right).S\left(s^{-1}W_n^Y(s)^2\right)}$‘ (12).

With S as the smoothing operator and s as the scale, WCOH serves as a localized correlation coefficient in the time–frequency space.

4. Results

4.1. Assessment of Drought Occurrence on the Basin

Drought analysis was performed for each meteorological station using the SPEI index at 1-, 3-, 6-, 9-, 12-, and 24-month timescales using precipitation and temperature data from the meteorological stations. Also, drought duration and severity were determined using run theory. Run theory provides a straightforward and efficient approach to detecting and examining drought events (Deger et al., 2023; Guerrero-Salazar et al., 1975). Figure 2 shows a time series at different time scales using all meteorological stations. In addition, Fig. 3 are generated a heat map illustrating the basin at various time scales using the mean SPEI data for the basin.

Historical droughts at different time scales have been examined when considering the drought risk assessment in the Kızılırmak Basin as given in both Fig. 2 and Fig. 3. As seen in both figures, severe droughts have become more frequent and intense, particularly since 2015, with previous peaks in the 1950s, 1960s, and 2000s. However, the year of the highest peaks is better illustrated in Fig. 2. The years in which the most severe droughts occurred varied depending on the time scale. For instance, while severe droughts were observed in the early 2000s for 1- and 3-month time scales, they were more prominent in the years following 2020 for 6-, 9-, 12-, and 24-month time scales. Based on the historical drought patterns in this particular basin, projections suggest an increased likelihood of prolonged and intense drought events from 2020 onward.

Figure 4 presents the results of the wavelet power spectrum and global wavelet spectrum analyses for the SPEI at three distinct temporal scales: SPEI 1 (monthly), SPEI 3 (seasonal), and SPEI 12 (annual). These analyses are based on the mean SPEI values calculated from all monitoring stations across the basin. Wavelet analysis serves as a sophisticated method for examining localized power fluctuations within time-series data. This technique breaks down the time series into a time–frequency domain, enabling the identification of primary variability patterns and their temporal evolution (Belayneh et al., 2016; Karbasi et al., 2022). The color scale represents the strength of the wavelet transform, with red and yellow indicating areas of higher intensity

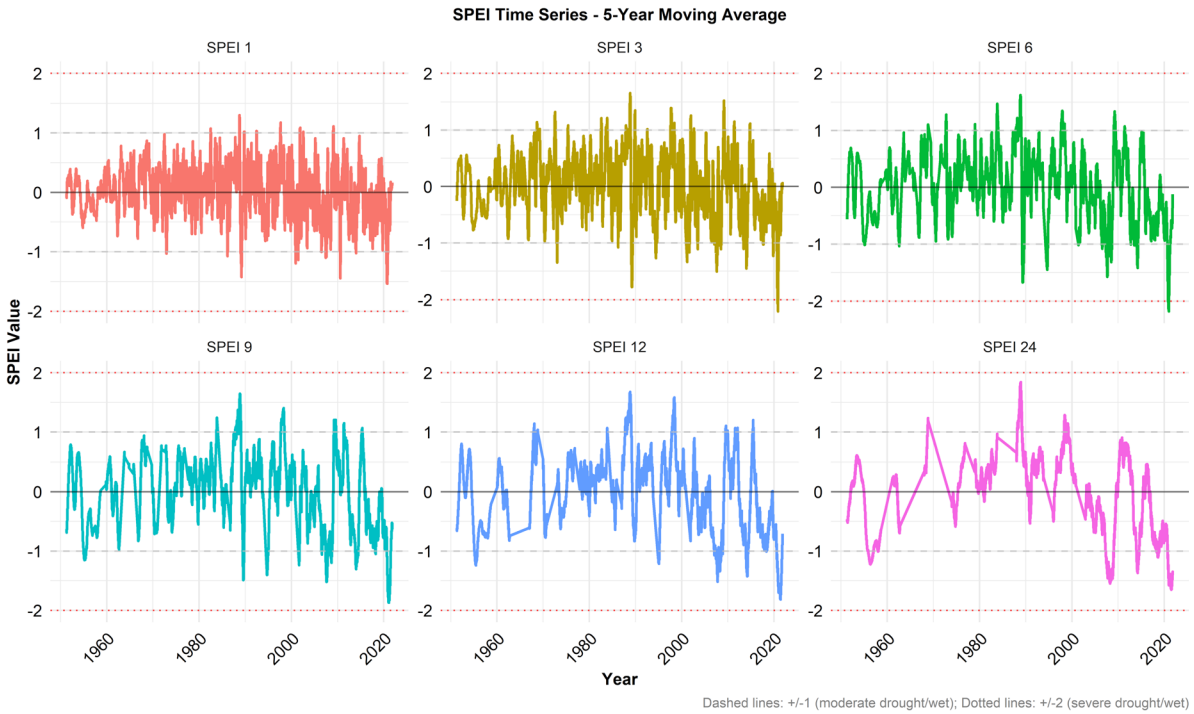

Fig. 2
Time series at different time scales of the SPEI index for all stations considered as 5-year moving average in the Kızılırmak Basin

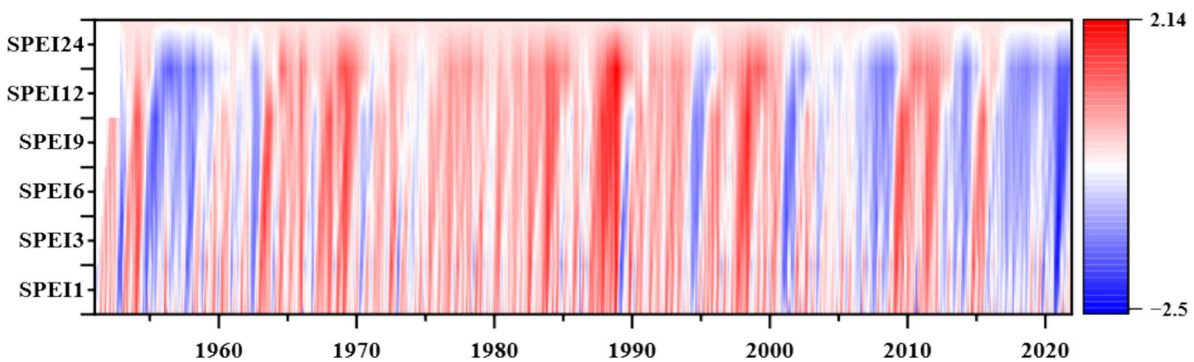

Fig. 3
Heat map of the Kızılırmak Basin utilized using average SPEI values at different time scales

(left panel). Also, Contours delineate areas where the wavelet power is statistically significant with a 95% confidence level. Right panel red areas highlight regions where the wavelet power is significantly greater than the background noise at the 95% confidence level. The wavelet power spectrum for the monthly analysis (SPEI 1) demonstrates pronounced fluctuations at multiple time scales. The global wavelet spectrum identifies prominent periodicities that may be related to short-term climate variability or hydrological phenomena. Seasonal analysis (SPEI 3) reveals distinct periodicities potentially linked to seasonal and climatic basin influences. The power spectrum's significant areas emphasize the dominant periods of these cycles. The wavelet power spectrum of the annual analysis (SPEI 12) highlights

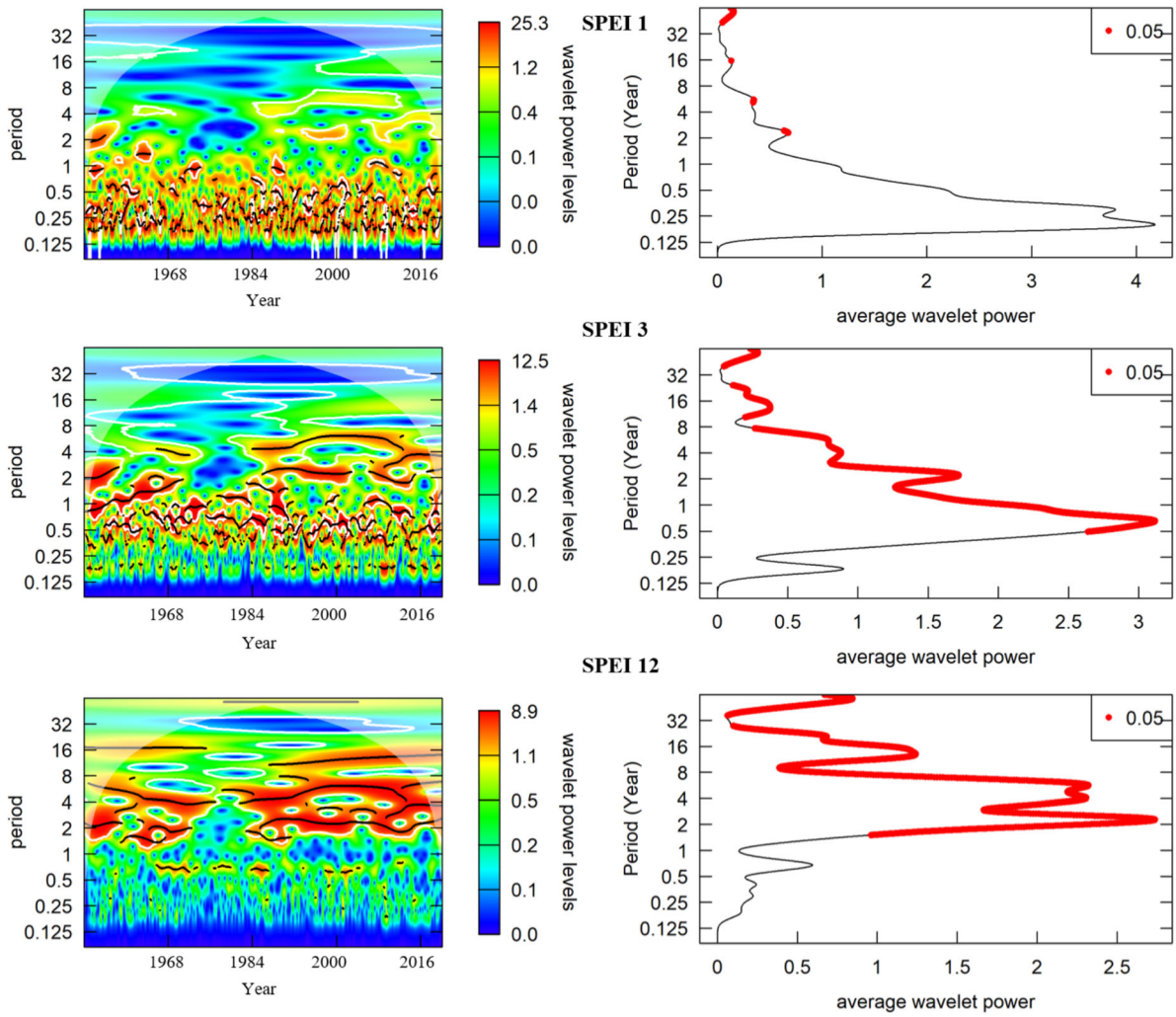

Fig. 4
The wavelet power spectrum (left panel) and the global wavelet spectrum (right panel) analysis of mean SPEI for three different timescales: (first row) SPEI 1 (monthly), (second row) SPEI 3 (seasonal), and (third row) SPEI 12 (annual) time scales

long-term climatic influences and patterns within the basin. Prominent peaks in the global wavelet spectrum indicate the importance of multi-year cycles, potentially linked to large-scale climate drivers, on the basin's hydrology.

4.2. *Assessment of Atmospheric-Ocean Climate Indices*

This study examined several climate indices, including the North Atlantic Oscillation (NAO), Niño 1.2, Niño 3, Niño 3.4, Niño 4, Atlantic Multidecadal Oscillation (AMO), Pacific Decadal Oscillation (PDO), Oceanic Niño Index (ONI), and Southern Oscillation Index (SOI). Figure 5 depicts the time series of atmospheric and oceanic climate indices used within the scope of this study. Each index represents atmospheric or oceanic conditions in a specific region and illustrates how these conditions have changed over time. In these graphs, positive and negative anomalies for each index are represented by distinct colors (e.g., positive anomalies in orange, negative anomalies in blue). This allows for a clearer visualization of the changes in climate indices over

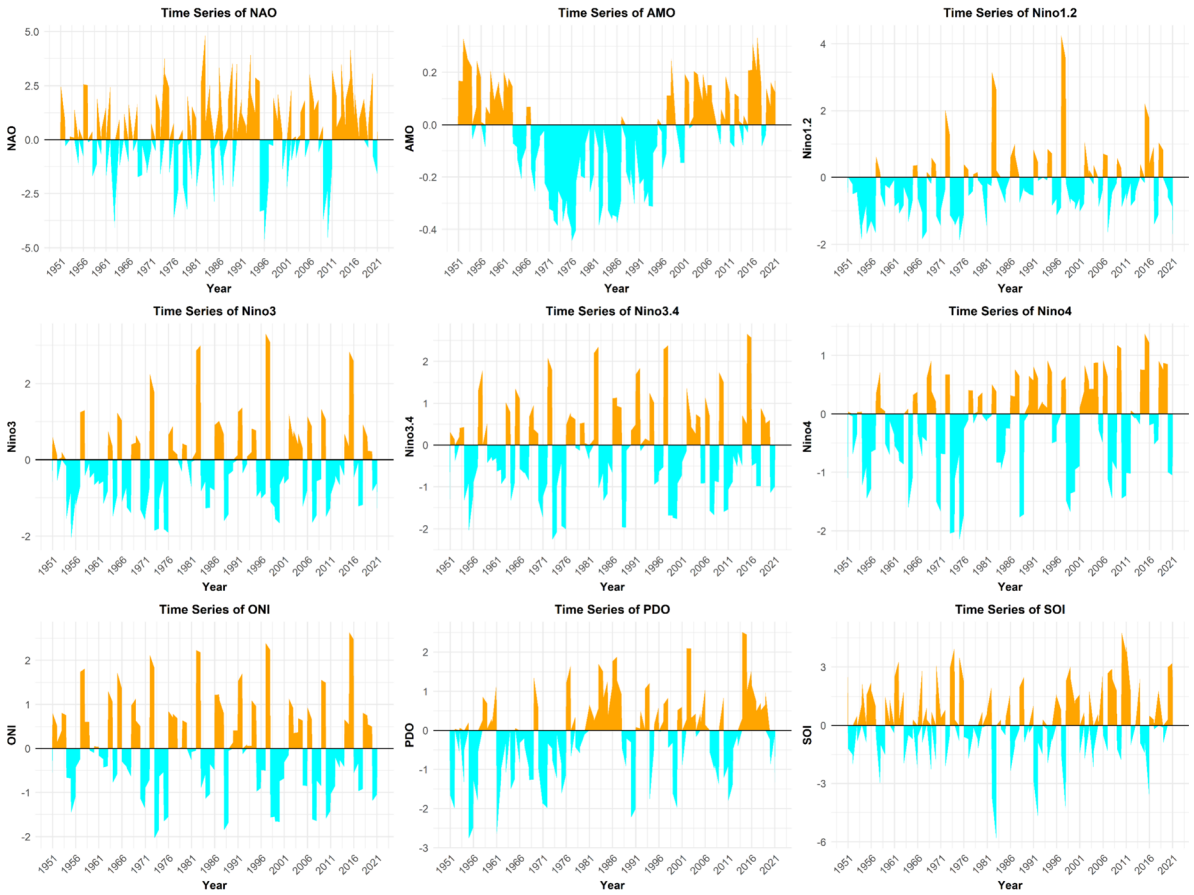

Fig. 5
Time Series of Atmospheric-Ocean Climate Indices Used in This Study: Analysis of NAO, AMO, Nino1.2, Nino3, Nino3.4, Nino4, ONI, PDO, and SOI Indices

time and the identification of extreme events. The climate indices and their associated data sources used in this research are obtained from the NOAA Physical Sciences Laboratory (PSL) (link: https://psl.noaa.gov/data/climateindices/list/). A summary of climate indices is in Abdelkader and Yerdelen (2022).

4.3. *Examining the Relationship of Drought Occurrence to Atmospheric and Oceanic Climate Indices*

We examined correlations between SPEI-12 and atmosphere-ocean climate indices for simultaneous and one-year lag periods to assess potential climate-drought relationships. One-year lag analysis compared the previous year's climate index values to current year SPEI-12. Correlation coefficients are mapped across the region with star (*) indicating statistical significance at the 95% level. Figure 6 reveals that correlation magnitudes are consistently weak, ranging from approximately -0.15 to +0.15 across all climate indices. NAO, AMO, and SOI exhibit predominantly negative correlations with SPEI-12, while Niño indices (1+2, 3, 3.4, 4), ONI, and PDO show positive correlations. However, these weak correlations indicate that climate modes collectively explain less than 2-3% of SPEI variance in the basin. The spatial patterns show considerable heterogeneity, with neighboring stations frequently displaying contrasting correlation signs and significance levels, suggesting that local factors dominate over large-scale climate influences.

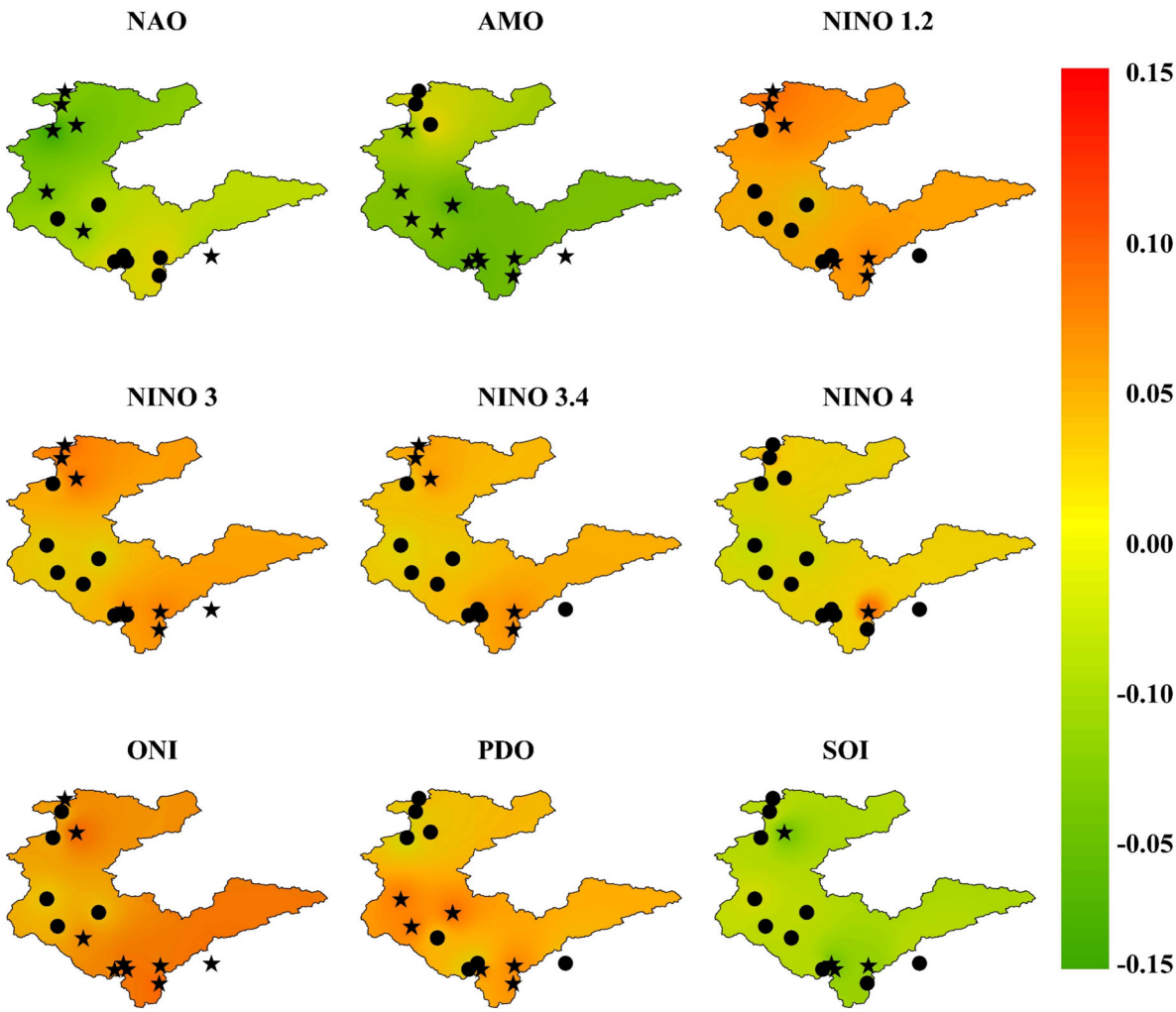

Fig. 6
Spatial distribution of Pearson correlation between SPEI 12 and Atmospheric-Ocean climate indices in the same year. A star (*) indicates correlations that are significant at the 95% confidence level

Figure 7 depicts the spatial correlation between SPEI-12 and several atmospheric-oceanic climate indices for a one-year lead time. The SOI indices exhibit significant correlations across multiple regions, suggesting robust predictive power for future drought conditions. The Nino 1 + 2, Nino 3, Nino 4, and ONI indices demonstrate moderate correlations with notable spatial patterns, indicating potential inverse relationships with future drought. While the NAO index shows weaker but still significant correlations, its predictive capability for drought is less pronounced. Overall, the SOI emerges as the most prominent predictor of future drought, while the AMO, PDO, and particularly Nino 4 exhibit inverse relationships.

Figure 8 shows cross-correlation plots between different SPEI timescales (1, 3, 6, 9, 12, and 24 months) and various atmospheric-oceanic climate indices. The plots also reveal potential lagged relationships between SPEI and the climate indices. A positive lag indicates that changes in the climate index precede changes in SPEI, while a negative lag suggests the opposite. Drought occurrences are investigated at different periods such as short-term

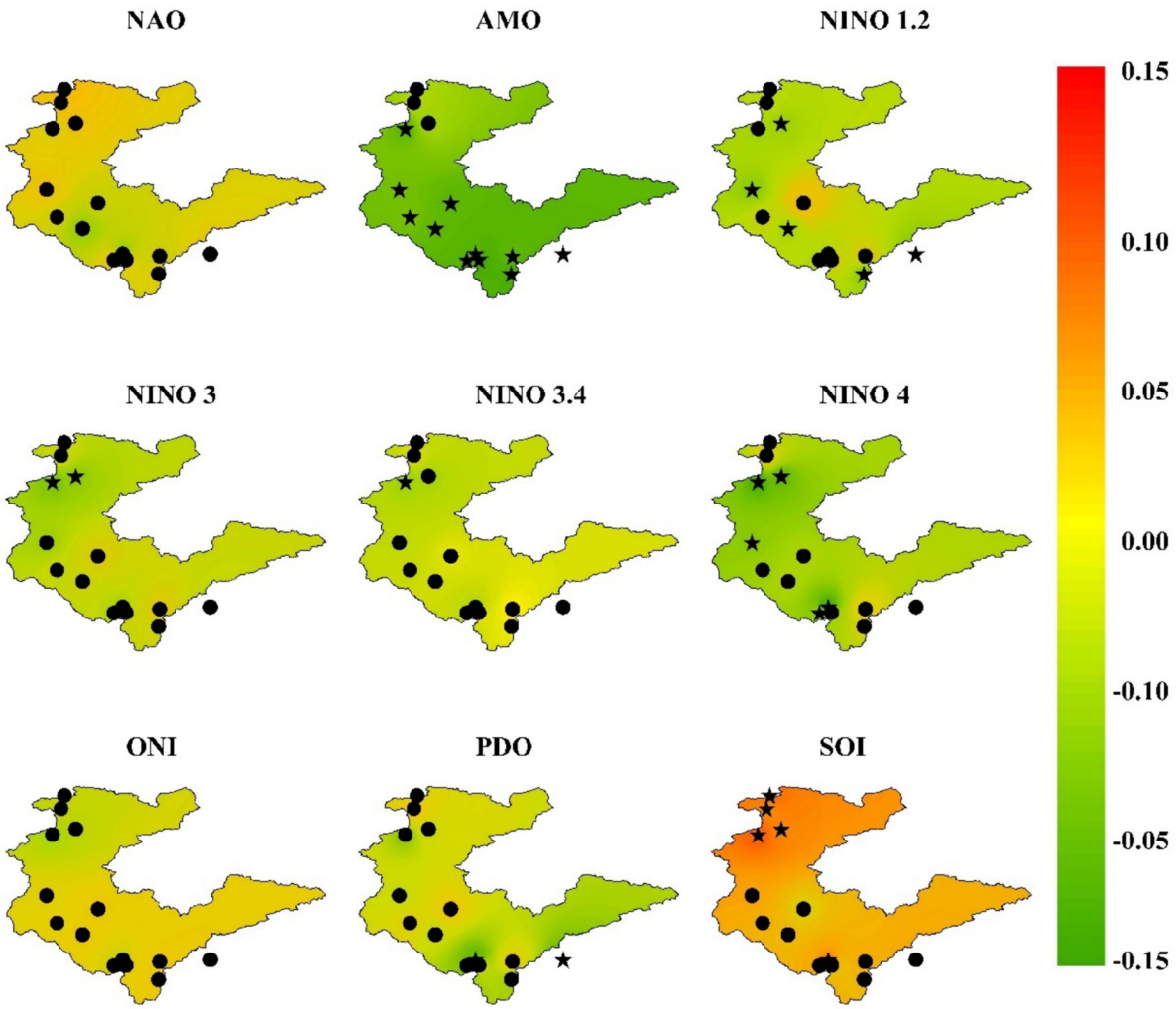

Fig. 7
Spatial distribution of Pearson correlation between SPEI 12 and Atmospheric-Ocean climate indices in the one year ahead. A star (*) indicates correlations that are significant at the 95% confidence level

predictions (1–3 months), medium-term predictions (3–12 months), and Long-term predictions (12–24 months). According to Fig. 8, ENSO-related indices (Niño 1 + 2, Niño 3, Niño 4, ONI) show the strongest positive correlations, peaking around 0–5 months lead time at SPEI 1. In addition, PDO shows a moderate positive correlation, slightly lagging behind (12-month lag) ENSO indices. However, NAO, SOI, and AMO show weak, mostly negative correlations.

Compared to the SPEI 1 time scale, the SPEI 3-time scale exhibits stronger and more sustained positive relationships with ENSO indices and the ONI. The Niño 3 and ONI indices show the most pronounced correlations, closely trailed by Niño 4 and Niño 1 + 2. The PDO correlation gets stronger and more in sync with ENSO at the 3-month scale. AMO, NAO, and SOI are weak and mostly negative. ENSO indices and ONI are strongly positive, and the broader peaks show more persistence at the 6-month scale. Niño 3 and ONI are the leading indicators followed by Niño 4. PDO correlation gets stronger and almost matches ENSO indices. AMO is slightly

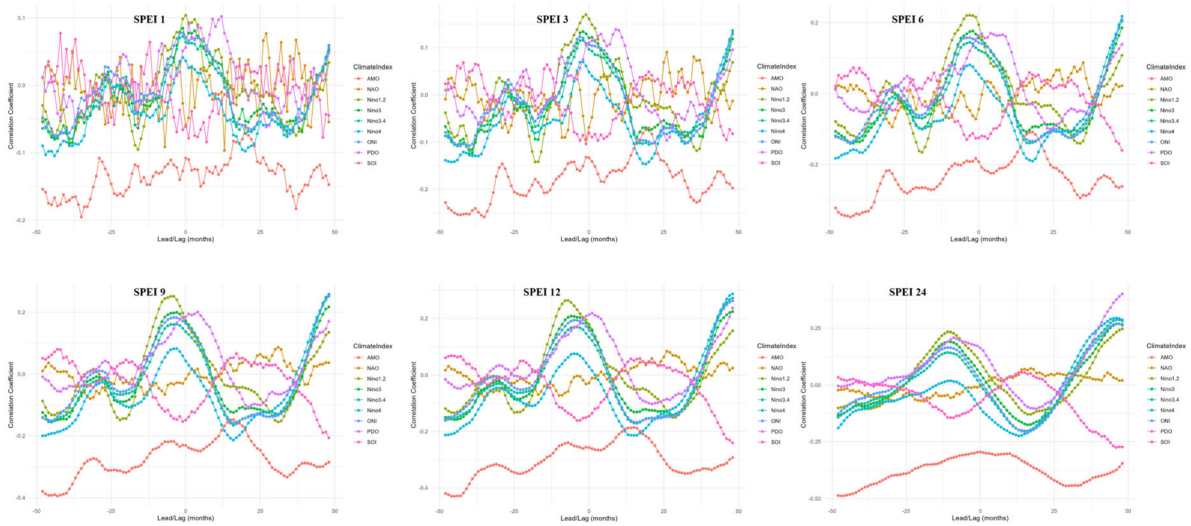

Fig. 8
The cross-correlation between an SPEI time scale (1, 3, 6, 9, 12, or 24 months) and various atmospheric-ocean climate indices. The x-axis shows the lag in months, and the y-axis represents the correlation coefficient

better but still weak. NAO and SOI are weak and mostly negative.

At the SPEI 9-month timescale, ENSO indices, ONI, and PDO are very highly correlated and positive, so their influence is strong. The different Niño regions are not as distinct, so it's a more general ENSO effect. AMO is more correlated and has a unique pattern, positive at longer lead times. NAO is still weak but shows some positive values at longer lead times. SOI is strongly negative, as expected. At the SPEI 12-month timescale, ENSO indices, ONI, and PDO are highly correlated and positive, so their influence is strong. AMO is more correlated and has a pattern that is negative at both long lead and lag times. NAO is slightly better but still the weakest correlated index. SOI is negative and mirrors the ENSO indices, as expected. At the SPEI 24-month timescale, ENSO indices (Niño 3, Niño 4, and ONI) are the most highly correlated, especially at 10–20 month lead times. PDO is also positive but weaker than the ENSO indices. NAO is weak and mostly negative. The SOI maintains its negative correlation pattern, as expected given its inverse relationship with ENSO. Importantly, the AMO exhibits a consistently negative correlation across all lead and lag times, a crucial observation previously overlooked.

Figure 9 illustrates the cross-wavelet transform (XWT) relationship between the 12-month Standardized Precipitation Evapotranspiration Index (SPEI) considering mean all stations and various atmospheric-oceanic climate indices. The relationship between SPEI and large-scale climate indices varies considerably. **SPEI and AMO:** A generally weak coherence characterizes the relationship between SPEI and the Atlantic Multidecadal Oscillation (AMO). While some intermittent periods of significant coherence exist, they are sporadic. Notably, a slightly stronger coherence is observed within the 16–32 month band, with prominent periods during the 1960s and late 1990s to early 2000s. Importantly, the phase relationship between these two indices is predominantly negative, as indicated by leftward-pointing arrows, implying that they tend to move in opposite directions. **SPEI and NAO:** In contrast to the AMO, the SPEI exhibits a stronger coherence with the North Atlantic Oscillation (NAO), especially at longer time scales between 32 and 64 months. Significant coherence is evident across much of the time series for periods exceeding 32 months. Unlike the SPEI-AMO relationship, the SPEI and NAO tend to be in phase, as shown by rightward-pointing arrows, suggesting a positive correlation.

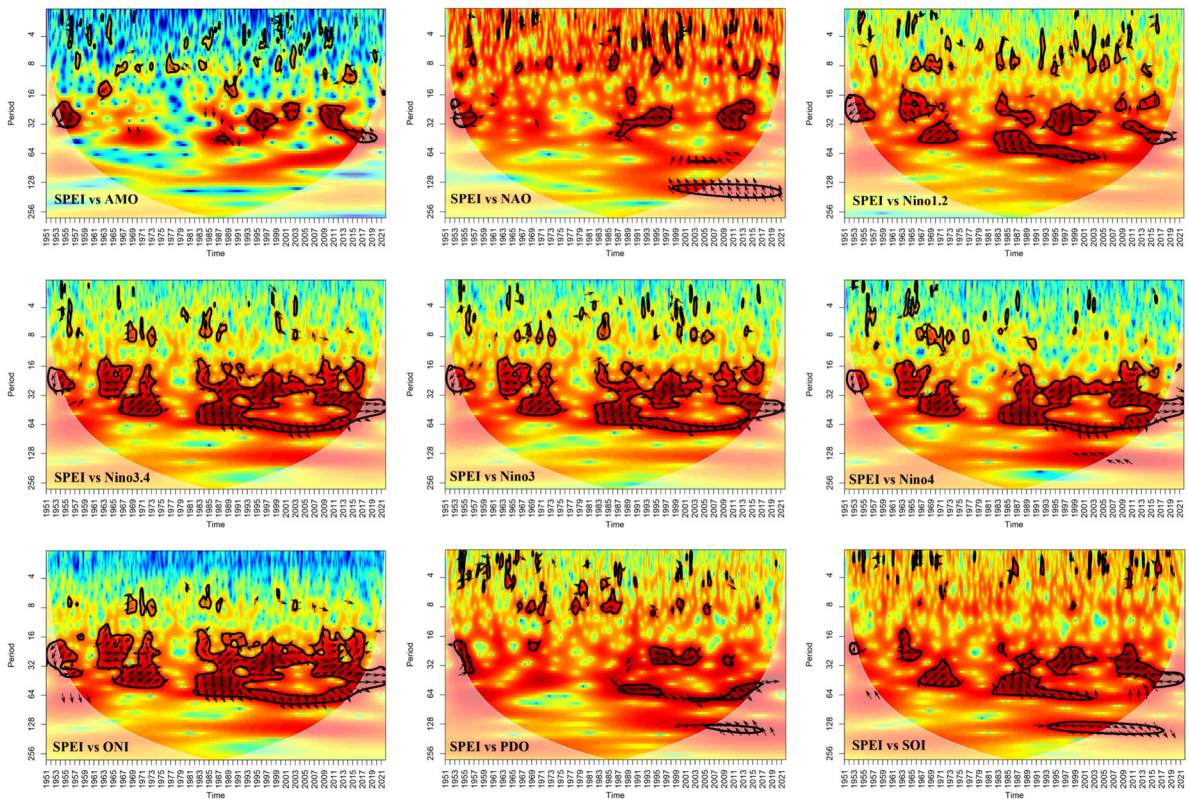

Fig. 9
Cross-wavelet transform (XWT) between SPEI 12-month time scale and the atmospheric-ocean climate indices

The relationship between SPEI and the El Niño-Southern Oscillation (ENSO) indices is notably robust. **SPEI and Niño indices (1.2, 3.4, 3, 4):** All Niño indices exhibit strong and persistent coherence with SPEI, particularly within the 16–64 month band. Significant coherence clusters are evident in the 1960s, 1980s, and 1990s-2000s. A consistently in-phase relationship between SPEI and these indices is observed, indicating a strong positive correlation. **SPEI and ONI:** Similar to the Niño indices, the ONI displays a very strong and persistent coherence with SPEI across multiple timescales. This relationship is characterized by a consistent in-phase pattern, signifying a robust positive correlation. **SPEI and PDO:** The Pacific Decadal Oscillation (PDO) shows strong coherence with SPEI, especially at longer periods (32–64 months). Significant coherence is observed throughout most of the time series. While the overall relationship is in phase, some variability in the phase relationship is evident. **SPEI and SOI:** The Southern Oscillation Index (SOI) exhibits a strong coherence with SPEI, particularly within the 16–64 month band. Significant coherence clusters coincide with those of the ENSO indices. However, unlike the ENSO indices and PDO, the SOI is consistently out of phase with SPEI, indicated by leftward-pointing arrows, suggesting a negative correlation. This negative relationship is expected given the inverse relationship between SOI and ENSO.

5. Discussion

This study investigated the complex interplay between major atmospheric-oceanic oscillation indices and drought conditions within Türkiye's vital Kızılırmak Basin. By employing the SPEI at various timescales and utilizing both correlation and cross-

wavelet analyses, this research provides a comprehensive understanding of drought dynamics and their teleconnections in the region.

The observed escalation in the frequency and intensity of drought events within the Kızılırmak Basin, particularly the pronounced increase since 2015, signals a critical hydroclimatic vulnerability. The recurrence of drought peaks in the 1950s, 1960s, and early 2000s indicates historical variability, yet the recent shift towards more prolonged durations (6–24 months) post-2020, following a prevalence of short-term droughts (1–3 months) in the early 2000s, suggests a potential long-term drying trend. This transition is highly concerning as prolonged water deficits pose significant challenges to the basin's vital agricultural sector, reservoir management, and overall water security. Our findings are consistent in the previous researches (Kurnaz, 2014; Tosunoglu et al., 2023; Türkeş & Erlat, 2003).

Moderate positive correlations were identified between SPEI-12 and ENSO indices (Niño 3.4, ONI) in the central and southern Kızılırmak Basin, with Pearson correlation coefficients ranging from 0.05 to 0.15. This suggests that El Niño conditions, typically associated with warmer equatorial Pacific Sea surface temperatures, tend to coincide with wetter periods in these sub-regions. While these coefficients indicate a statistically measurable influence, their relatively low magnitude highlights that ENSO is not the sole, dominant driver of drought variability in the Kızılırmak Basin but rather contributes as one factor within a complex system. For example, Singh et al. (2022) studied the risk of concurrent regional drought with ENSO variability. Climate indices are also used in some studies to investigate drought occurrences (Abiy et al., 2019; Guria et al., 2025; Zeleke et al., 2022).

Despite revealing significant teleconnections, it is crucial to acknowledge that the identified correlations and coherence levels indicate that these large-scale atmospheric oscillations explain only a portion of the total drought variability in the Kızılırmak Basin. This suggests that local and regional factors, such as topography, land use changes, anthropogenic water demands, and other mesoscale atmospheric phenomena, likely play equally, if not more, dominant roles in shaping the basin's complex drought dynamics.

This study utilized SPEI as a robust drought indicator, considering both precipitation and evapotranspiration; however, the availability of long-term, spatially dense climate data for all variables remains a challenge in some regions. Future research could benefit from integrating higher-resolution gridded datasets or reanalysis products to capture finer spatial variations in drought patterns and teleconnection impacts. Furthermore, while this study focused on the direct statistical relationships, future work could explore the physical mechanisms through which these teleconnections influence regional atmospheric circulation and moisture transport specifically over Türkiye, potentially using atmospheric modeling or more sophisticated causal inference techniques. Investigating the combined or compound effects of multiple teleconnections, as well as their interactions with climate change projections, would also provide a more holistic understanding for long-term drought preparedness and water resource planning in the Kızılırmak Basin.

6. Conclusion

This study investigated the impact of major atmospheric oscillations on drought conditions within Türkiye's critical Kızılırmak Basin. Specifically, the influence of the North Atlantic Oscillation (NAO), Niño indices (1.2, 3, 3.4, and 4), Atlantic Multidecadal Oscillation (AMO), Pacific Decadal Oscillation (PDO), Oceanic Niño Index (ONI), and Southern Oscillation Index (SOI) on drought events was examined. The Standardized Precipitation Evapotranspiration Index (SPEI) served as a drought indicator. Our findings are given as follows:

Analysis of historical drought patterns revealed an alarming trend of increased frequency and intensity, particularly since 2015, with recurring peaks in the 1950s, 1960s, and early 2000s. While short-term droughts (1–3 months) were prevalent in the early 2000s, longer-term droughts (6–24 months) intensified post-2020. These findings emphasize a growing risk of prolonged and severe droughts in the Kızılırmak Basin.

Moderate positive correlations were observed between SPEI-12 and ENSO indices (Niño 3.4, ONI)

at the same year, particularly in central and southern regions. For instance, the Pearson correlation coefficient for SPEI-12 and Niño 3.4 ranged from 0.05 to 0.15 across relevant sub-regions, suggesting a measurable but limited influence on drought occurrence. In contrast, NAO, AMO, and SOI exhibited negative correlations with SPEI-12. For example, NAO showed correlation coefficients between − 0.05 and − 0.15, indicating associations with wetter conditions. PDO and other Niño indices also influenced drought patterns, but their impact was less pronounced compared to Niño 3.4 and ONI. Lead-time analysis identified SOI as the most consistent predictor of SPEI-12, with significant correlations (e.g., correlation coefficients up to 0.05 to 0.15) across multiple regions.

Comparative analysis reveals a complex interplay of atmospheric-oceanic indices influencing SPEI variability across timescales. ENSO indices, particularly Niño 3 and ONI, dominate short-term SPEI fluctuations, while the PDO's influence grows with timescale. The medium-term sees comparable impacts from ENSO and PDO, with the AMO's role gradually increasing. Over the long term, AMO emerges as a weak driver, though ENSO and PDO remain influential. The NAO consistently exhibits weak correlations, suggesting a limited direct impact on SPEI in the region. The SOI maintains a consistent inverse relationship with ENSO indices across all timescales. As the timescale extends, correlation patterns become smoother and more persistent, reflecting the cumulative effects of climate processes.

ENSO-related indices (Niño3.4, Niño3, Niño4, and ONI) emerged as the primary drivers of SPEI-12 variability, demonstrating strong and consistent coherence (particularly within the 16–64-month band). A predominantly in-phase relationship indicates that El Niño conditions are associated with wetter periods, while La Niña events correspond to drier conditions. The PDO also significantly influences SPEI-12 (especially at 32–64-month periods), exhibiting strong coherence. In contrast, the SOI, while strongly correlated, is inversely related to SPEI-12. The NAO shows moderate coherence, especially at longer timescales, with a generally positive impact on SPEI-12, whereas the AMO's influence is weaker. Most indices exhibit strongest coherence at interannual to multi-year timescales (16–64 months), with varying degrees of influence across different decades.

Acknowledgements

The General Directorate of Meteorology (MGM) is to be acknowledged for its contributions to meteorological data.

Author Contribution M.I.Yuce: Revised manuscript, M. Esit: Provided data and wrote the manuscript, I. H. Deger and I. YASA: Observed analysis.

Funding

Not applicable.

Code Availability

No datasets were generated or analysed during the current study.

Data Availability

The data that support the findings of this study are available from the corresponding author upon request.

Declarations

Conflict of interest The authors declare no competing interests.

Ethical Approval Not applicable.

Consent to Participate Not applicable.

Consent for Publication Not applicable.

Informed Consent This study did not include any human participants or animals.

References

Abdelkader, M., & Yerdelen, C. (2022). Hydrological drought variability and its teleconnections with climate indices. *Journal of Hydrology, 605*, Article 127290. https://doi.org/10.1016/j.jhydrol.2021.127290

Abiy, A. Z., Melesse, A. M., Seyoum, W. M., & Abtew, W. (2019). Chapter 22 - Drought and climate teleconnection and drought monitoring. In A. M. Melesse, W. Abtew, & G. Senay (Eds.), *Extreme hydrology and climate variability* (pp. 275–295). Elsevier.

Abramowitz, M., & Stegun, I. A. (1968). *Handbook of mathematical functions with formulas, graphs, and mathematical tables*. Government Printing Office.

Afshar, M. H., Şorman, A. Ü., Tosunoğlu, F., et al. (2020). Climate change impact assessment on mild and extreme drought events using copulas over Ankara, Turkey. *Theoretical and Applied Climatology, 141*, 1045–1055. https://doi.org/10.1007/s00704-020-03257-6

AghaKouchak, A., Farahmand, A., Melton, F. S., et al. (2015). Remote sensing of drought: Progress, challenges and opportunities. *Reviews of Geophysics, 53*, 452–480. https://doi.org/10.1002/2014RG000456

Aghelpour, P., Bahrami-Pichaghchi, H., Varshavian, V., & Norooz-Valashedi, R. (2023). Evaluating the predictability of eight Atmospheric-Oceanic signals affecting Iran's Droughts, employing intelligence based and stochastic methods. *Advances in Space Research, 71*, 2394–2415. https://doi.org/10.1016/j.asr.2022.10.047

Akturk, G., Zeybekoglu, U., & Yildiz, O. (2022). Assessment of meteorological drought analysis in the Kizilirmak River Basin, Turkey. *Arabian Journal of Geosciences, 15*, 850. https://doi.org/10.1007/s12517-022-10119-0

Arslan, O., Bilgil, A., & Veske, O. (2016). Standart yağiş indisi yöntemi ile kizilirmak havzasi'nin meteorolojik kuraklik analizi. *NOHU Journal of Engineering Sciences, 5*, 188–194. https://doi.org/10.28948/ngumuh.295572

Baltacı, H., Akkoyunlu, B. O., & Tayanç, M. (2018). Relationships between teleconnection patterns and Turkish climatic extremes. *Theoretical and Applied Climatology, 134*, 1365–1386. https://doi.org/10.1007/s00704-017-2350-z

Belayneh, A., Adamowski, J., & Khalil, B. (2016). Short-term SPI drought forecasting in the Awash River Basin in Ethiopia using wavelet transforms and machine learning methods. *Sustainable Water Resources Management, 2*, 87–101. https://doi.org/10.1007/s40899-015-0040-5

Benesty, J., Chen, J., Huang, Y., & Cohen, I. (2009). Pearson correlation coefficient. In I. Cohen, Y. Huang, J. Chen, & J. Benesty (Eds.), *Noise reduction in speech processing* (pp. 1–4). Springer.

Chylek, P., Dubey, M. K., Lesins, G., et al. (2014). Imprint of the Atlantic multi-decadal oscillation and Pacific decadal oscillation on southwestern US climate: Past, present, and future. *Climate Dynamics, 43*, 119–129. https://doi.org/10.1007/s00382-013-1933-3

Citakoglu, H., & Minarecioglu, N. (2021). Trend analysis and change point determination for hydro-meteorological and groundwater data of Kizilirmak basin. *Theoretical and Applied Climatology, 145*, 1275–1292. https://doi.org/10.1007/s00704-021-03696-9

Danandeh Mehr, A., & Vaheddoost, B. (2020). Identification of the trends associated with the SPI and SPEI indices across Ankara, Turkey. *Theoretical and Applied Climatology, 139*, 1531–1542. https://doi.org/10.1007/s00704-019-03071-9

Deger, İH., Yüce, M. İ, & Eşit, M. (2023). An investigation of hydrological drought characteristics in Kızılırmak Basin, Türkiye: Impacts and trends. *Bitlis Eren Üniversitesi Fen Bilimleri Dergisi, 12*, 126–139. https://doi.org/10.17798/bitlisfen.1200742

Duzenli, E., Tabari, H., Willems, P., & Yilmaz, M. T. (2018). Decadal variability analysis of extreme precipitation in Turkey and its relationship with teleconnection patterns. *Hydrological Processes, 32*, 3513–3528. https://doi.org/10.1002/hyp.13275

Esit, M., Kumar, S., Pandey, A., et al. (2021). Seasonal to multi-year soil moisture drought forecasting. *Npj Climate and Atmospheric Science, 4*, 1–8. https://doi.org/10.1038/s41612-021-00172-z

Fan, L., Wang, Y., Cao, C., & Chen, W. (2024). Teleconnections of atmospheric circulations to meteorological drought in the Lancang-Mekong River Basin. *Atmosphere, 15*, 89. https://doi.org/10.3390/atmos15010089

Ghasemi, P., Karbasi, M., Zamani Nouri, A., et al. (2021). Application of Gaussian process regression to forecast multi-step ahead SPEI drought index. *Alexandria Engineering Journal, 60*, 5375–5392. https://doi.org/10.1016/j.aej.2021.04.022

Gu, Z., Gu, L., Yin, J., et al. (2024). Impact of atmospheric circulations on droughts and drought propagation over China. *Science China Earth Sciences*. https://doi.org/10.1007/s11430-023-1329-x

Guerrero-Salazar PLA, Yevjevich VM, Colorado State University P (1975) Analysis of drought characteristics by the theory of runs

Gultepe, I., Heymsfield, A. J., Field, P. R., & Axisa, D. (2017). Ice-phase precipitation. *Meteorological Monographs, 58*, 6–1.

Gultepe, I., Agelin-Chaab, M., Komar, J., et al. (2019). A meteorological supersite for aviation and cold weather applications. *Pure and Applied Geophysics, 176*, 1977–2015. https://doi.org/10.1007/s00024-018-1880-3

Gumus, V. (2023). Evaluating the effect of the SPI and SPEI methods on drought monitoring over Turkey. *Journal of Hydrology, 626*, Article 130386. https://doi.org/10.1016/j.jhydrol.2023.130386

Guria, R., Dwivedi, S., Nayak, P., et al. (2025). A comprehensive 120-year assessment of drought dynamics and climate teleconnections in Odisha, India (1901–2020): Insights from SPI and trend evaluation. *Natural Hazards*. https://doi.org/10.1007/s11069-025-07336-7

Hamal, K., Sharma, S., Pokharel, B., et al. (2021). Changing pattern of drought in Nepal and associated atmospheric circulation. *Atmospheric Research, 262*, Article 105798. https://doi.org/10.1016/j.atmosres.2021.105798

Hao, Z., & AghaKouchak, A. (2013). Multivariate standardized drought index: A parametric multi-index model. *Advances in*

Water Resources, 57, 12–18. https://doi.org/10.1016/j.advwatres.2013.03.009

He, N., Yin, J., Slater, L. J., et al. (2024). Global terrestrial drought and its projected socioeconomic implications under different warming targets. *Science of the Total Environment, 946*, Article 174292. https://doi.org/10.1016/j.scitotenv.2024.174292

Karbasi, M., Karbasi, M., Jamei, M., et al. (2022). Development of a new wavelet-based hybrid model to forecast multi-scalar SPEI drought index (case study: Zanjan city, Iran). *Theoretical and Applied Climatology, 147*, 499–522. https://doi.org/10.1007/s00704-021-03825-4

Kebapcioğlu, E., & Partal, T. (2024). Tele-connections of atmospheric oscillations on streamflow data in Turkey. *Meteorology and Atmospheric Physics, 136*, 20. https://doi.org/10.1007/s00703-024-01014-2

Kömüşcü, A. Ü., & Aksoy, M. (2024). Characterizing variability of spatial patterns of annual and seasonal precipitation of Turkey and identifying the probable driving factors including teleconnection patterns. *Journal of Water and Climate Change, 15*, 1392–1416. https://doi.org/10.2166/wcc.2024.665

Kurnaz L (2014) Drought in Turkey. İstanbul Policy Center, Sabancı Üniversitesi-İstanbul

Li, L., She, D., Zheng, H., et al. (2020). Elucidating diverse drought characteristics from two meteorological drought indices (SPI and SPEI) in China. *Journal of Hydrometeorology*. https://doi.org/10.1175/JHM-D-19-0290.1

Liu, Z., & Di Lorenzo, E. (2018). Mechanisms and predictability of pacific decadal variability. *Current Climate Change Reports, 4*, 128–144. https://doi.org/10.1007/s40641-018-0090-5

Manzano, A., Clemente, M. A., Morata, A., et al. (2019). Analysis of the atmospheric circulation pattern effects over SPEI drought index in Spain. *Atmospheric Research, 230*, Article 104630. https://doi.org/10.1016/j.atmosres.2019.104630

Matyasovszky, I. (2003). The relationship between NAO and temperature in Hungary and its nonlinear connection with ENSO. *Theoretical and Applied Climatology, 74*, 69–75. https://doi.org/10.1007/s00704-002-0697-1

McKee, T. B., Doesken, N. J., & Kleist, J. (1993). The relationship of drought frequency and duration to time scales. *Boston, MA: American Meteorological Society, 17*, 179–183.

Meresa, H., Zhang, Y., Tian, J., & Abrar Faiz, M. (2023). Understanding the role of catchment and climate characteristics in the propagation of meteorological to hydrological drought. *Journal of Hydrology, 617*, Article 128967. https://doi.org/10.1016/j.jhydrol.2022.128967

Mishra, A. K., & Singh, V. P. (2010). A review of drought concepts. *Journal of Hydrology, 391*, 202–216. https://doi.org/10.1016/j.jhydrol.2010.07.012

Mohammadrezaei, M., Soltani, S., & Modarres, R. (2020). Evaluating the effect of ocean-atmospheric indices on drought in Iran. *Theoretical and Applied Climatology, 140*, 219–230. https://doi.org/10.1007/s00704-019-03058-6

Mohammadrezaei, M., Soltani, S., & Modares, R. (2023). Investigation of the relationship of NINO4 and NAO indices with meteorological drought in synoptic stations in northern Iran. *Water and Soil Science., 33*, 135–150. https://doi.org/10.22034/ws.2021.48311.2441

Molla, M. (2020). Teleconnections between ocean-atmosphere coupled phenomenon and droughts in Tigray Region: Northern Ethiopia. *American Journal of Climate Change, 9*, 274–296. https://doi.org/10.4236/ajcc.2020.93018

Murgulet, D., Valeriu, M., Hay, R. R., et al. (2017). Relationships between sea surface temperature anomalies in the Pacific and Atlantic Oceans and South Texas precipitation and streamflow variability. *Journal of Hydrology, 550*, 726–739. https://doi.org/10.1016/j.jhydrol.2017.05.041

NASA Earth Observatory (2021) Turkey Experiences Intense Drought. https://earthobservatory.nasa.gov/images/147811/turkey-experiences-intense-drought. Accessed 19 Jan 2021

Ndehedehe, C. (2022). Droughts and impacts of climate teleconnections. In C. Ndehedehe (Ed.), *Satellite remote sensing of terrestrial hydrology* (pp. 441–487). Springer International Publishing.

Nejadrekabi, M., Eslamian, S., & Zareian, M. J. (2022). Spatial statistics techniques for SPEI and NDVI drought indices: A case study of Khuzestan Province. *International Journal of Environmental Science and Technology, 19*, 6573–6594. https://doi.org/10.1007/s13762-021-03852-8

Nourani, V., Najafi, H., Sharghi, E., & Roushangar, K. (2021). Application of Z-numbers to monitor drought using large-scale oceanic-atmospheric parameters. *Journal of Hydrology, 598*, Article 126198. https://doi.org/10.1016/j.jhydrol.2021.126198

Oñate-Valdivieso, F., Uchuari, V., & Oñate-Paladines, A. (2020). Large-scale climate variability patterns and drought: a case of study in South–America. *Water Resources Management, 34*, 2061–2079. https://doi.org/10.1007/s11269-020-02549-w

Öztürk, D. S., Keskin, A. Ü., & Zeybekoğlu, U. (2023). Meteorological and hydrological drought analysis of The Kızılırmak Basin. *Black Sea Journal of Agriculture, 6*, 427–438. https://doi.org/10.47115/bsagriculture.1307148

Palmer WC (1965) Meteorological Drought. U.S. Department of Commerce, Weather Bureau

Pei, Z., Fang, S., Wang, L., & Yang, W. (2020). Comparative analysis of drought indicated by the SPI and SPEI at various timescales in inner Mongolia, China. *Water, 12*, 1925. https://doi.org/10.3390/w12071925

Peng, J., Dadson, S., Hirpa, F., et al. (2020). A pan-African high-resolution drought index dataset. *Earth System Science Data, 12*, 753–769. https://doi.org/10.5194/essd-12-753-2020

Qian, X.-Y., Liu, Y.-M., Jiang, Z.-Q., et al. (2015). Detrended partial cross-correlation analysis of two nonstationary time series influenced by common external forces. *Physical Review E, 91*, Article 062816. https://doi.org/10.1103/PhysRevE.91.062816

Rezaei, A. (2023). Teleconnections between ocean–atmosphere circulations and historical integrated drought in the Middle East and North Africa. *Environmental Monitoring and Assessment, 195*, 775. https://doi.org/10.1007/s10661-023-11386-4

Robleh, H. B., Yuce, M. I., Esit, M., & Deger, I. H. (2024). Meteorological drought monitoring in Kızılırmak Basin, Türkiye. *Environmental Earth Sciences, 83*, 265. https://doi.org/10.1007/s12665-024-11550-0

Sagarika, S., Kalra, A., & Ahmad, S. (2015). Interconnections between oceanic–atmospheric indices and variability in the U.S. streamflow. *Journal of Hydrology, 525*, 724–736. https://doi.org/10.1016/j.jhydrol.2015.04.020

Sezen, C. (2024). Analysing the effects of atmospheric teleconnections on streamflow regime in the Eastern Black Sea Basin in Türkiye. *Doğal Afetler Ve Çevre Dergisi, 10*, 365–381. https://doi.org/10.21324/dacd.1422683

Shukla, S., & Wood, A. W. (2008). Use of a standardized runoff index for characterizing hydrologic drought. *Geophysical Research Letters*. https://doi.org/10.1029/2007GL032487

Singh, J., Ashfaq, M., Skinner, C. B., et al. (2022). Enhanced risk of concurrent regional droughts with increased ENSO variability and warming. *Nature Clinical Practice Endocrinology and Metabolism, 12*, 163–170. https://doi.org/10.1038/s41558-021-01276-3

Sureh, F. S., Sattari, M. T., Rostamzadeh, H., & Kahya, E. (2024). Meteorological drought assessment and prediction in association with combination of atmospheric circulations and meteorological parameters via rule based models. *Journal of Agricultural Sciences - Tarım Bilimleri, 30*, 61–78. https://doi.org/10.15832/ankutbd.1067486

Terzi, Ö., & İlker, A. (2021). Yağış Verilerinin Trend Analizi: Kızılırmak Havzası Örneği. *APJES, 9*, 371–377. https://doi.org/10.21541/apjes.735378

Thornthwaite, C. W. (1948). An approach toward a rational classification of climate. *Geographical Review, 38*, 55–94. https://doi.org/10.2307/210739

Tirivarombo, S., Osupile, D., & Eliasson, P. (2018). Drought monitoring and analysis: Standardised Precipitation Evapotranspiration Index (SPEI) and Standardised Precipitation Index (SPI). *Physics and Chemistry of the Earth, Parts a/b/c, 106*, 1–10. https://doi.org/10.1016/j.pce.2018.07.001

Torrence C, Compo GP (1998) A practical guide to wavelet analysis

Torrence, C., & Webster, P. J. (1999). Interdecadal changes in the ENSO–monsoon system. *Journal of Climate, 12*, 2679–2690. https://doi.org/10.1175/1520-0442(1999)012%3c2679:ICITEM%3e2.0.CO;2

Tosunoglu, F., Kahya, E., & Ghorbani, M. A. (2023). Spatial and temporal linkages between large-scale atmospheric oscillations and hydrologic drought indices in Turkey. *Integrated drought management.* (Vol. 2). CRC Press.

Turan, E. S. (2017). Current situation about drought in Turkey. *Turjoem, 2*, 122–129.

Türkeş, M., & Erlat, E. (2003). Precipitation changes and variability in Turkey linked to the North Atlantic oscillation during the period 1930–2000. *International Journal of Climatology, 23*, 1771–1796. https://doi.org/10.1002/joc.962

Türkeş, M., & Erlat, E. (2005). Climatological responses of winter precipitation in Turkey to variability of the North Atlantic Oscillation during the period 1930–2001. *Theoretical and Applied Climatology, 81*, 45–69. https://doi.org/10.1007/s00704-004-0084-1

Türkeş, M. (2020). İklim değişikliğinin tarimsal üretim ve gida güvenliğine etkileri: bilimsel bir değerlendirme. *Ege Coğrafya Dergisi, 29*(1), 125–149.

Ullah, I., Ma, X., Yin, J., et al. (2023). Spatiotemporal characteristics of meteorological drought variability and trends (1981–2020) over South Asia and the associated large-scale circulation patterns. *Climate Dynamics, 60*, 2261–2284. https://doi.org/10.1007/s00382-022-06443-6

Vazifehkhah, S., & Kahya, E. (2019). Hydrological and agricultural droughts assessment in a semi-arid basin: Inspecting the teleconnections of climate indices on a catchment scale. *Agricultural Water Management, 217*, 413–425. https://doi.org/10.1016/j.agwat.2019.02.034

Vicente-Serrano, S. M., Beguería, S., & López-Moreno, J. I. (2010). A multiscalar drought index sensitive to global warming: The standardized precipitation evapotranspiration index. *Journal of Climate, 23*, 1696–1718. https://doi.org/10.1175/2009JCLI2909.1

Wang, T., Tu, X., Singh, V. P., et al. (2023). A CMIP6-based framework for propagation from meteorological and hydrological droughts to socioeconomic drought. *Journal of Hydrology, 623*, Article 129782. https://doi.org/10.1016/j.jhydrol.2023.129782

Wilhite, D. (2000). *Chapter 1 Drought as a natural hazard: Concepts and definitions*. Drought Mitigation Center Faculty Publications.

Wilhite, D. A. (Ed.). (2005). *Drought and water crises: Science, technology, and management issues*. CRC Press.

Wilhite, D. A., & Glantz, M. H. (1985). Understanding: The drought phenomenon: The role of definitions. *Water International, 10*, 111–120. https://doi.org/10.1080/02508068508686328

Yang, R., & Xing, B. (2022). Teleconnections of large-scale climate patterns to regional drought in mid-latitudes: A case study in Xinjiang. *China. Atmosphere, 13*, 230. https://doi.org/10.3390/atmos13020230

Yang, Y., Gan, T. Y., & Tan, X. (2020). Spatiotemporal changes of drought characteristics and their dynamic drivers in Canada. *Atmospheric Research, 232*, Article 104695. https://doi.org/10.1016/j.atmosres.2019.104695

Yao, J., Tuoliewubieke, D., Chen, J., et al. (2019). Identification of drought events and correlations with large-scale ocean-atmospheric patterns of variability: A case study in Xinjiang, China. *Atmosphere, 10*, 94. https://doi.org/10.3390/atmos10020094

Yao, T., Zhao, Q., Wu, C., et al. (2024). Spatio-temporal variation characteristics of extreme climate events and their teleconnections to large-scale ocean-atmospheric circulation patterns in Huaihe River Basin, China during 1959–2019. *Chinese Geographical Science, 34*, 118–134. https://doi.org/10.1007/s11769-023-1398-1

Yılmaz, M., & Tosunoğlu, F. (2023). Assessing the main drivers of low flow series in Turkey. *Natural Hazards, 115*, 1927–1953. https://doi.org/10.1007/s11069-022-05621-3

Yuce, M. I., Deger, I. H., & Esit, M. (2023). Hydrological drought analysis of Yeşilırmak Basin of Turkey by streamflow drought index (SDI) and innovative trend analysis (ITA). *Theoretical and Applied Climatology*. https://doi.org/10.1007/s00704-023-04545-7

Zeleke, E. B., Melesse, A. M., & Kidanewold, B. B. (2022). Assessment of climate and catchment control on drought propagation in the Tekeze River Basin, Ethiopia. *Water, 14*, 1564. https://doi.org/10.3390/w14101564

Zhang, X., Miao, J., Wang, X., & Zhou, B. (2024). Interannual variation of summer compound hot and drought events in Xinjiang and its relationship with the north Atlantic sea surface temperature. *Journal of Climate*. https://doi.org/10.1175/JCLI-D-24-0086.1

Zhong, Y., Wang, B., Zou, C. B., et al. (2017). On the teleconnection patterns to precipitation in the eastern Tianshan Mountains, China. *Climate Dynamics, 49*, 3123–3139. https://doi.org/10.1007/s00382-016-3500-1

(Received November 26, 2024, revised June 13, 2025, accepted July 10, 2025)